Hindawi
Shock and Vibration
Volume 2018, Article ID 1737219, 12 pages
https://doi.org/10.1155/2018/1737219

Research Article

Alpha-Stable Distribution and Multifractal Detrended Fluctuation Analysis-Based Fault Diagnosis Method Application for Axle Box Bearings

Qing Xiong[1,2,3], **Weihua Zhang**[4], **Yanhai Xu**[3], **Yiqiang Peng**[1,2,3] and **Pengyi Deng**[3]

[1]*Key Laboratory of Fluid and Power Machinery, Ministry of Education, Xihua University, Chengdu, Sichuan 610039, China*
[2]*Key Laboratory of Automotive Measurement, Control and Safety, Xihua University, Chengdu, Sichuan 610039, China*
[3]*School of Automobile & Transportation, Xihua University, Chengdu, Sichuan 610039, China*
[4]*State Key Laboratory of Traction Power, Southwest Jiaotong University, Chengdu, Sichuan 610031, China*

Correspondence should be addressed to Yanhai Xu; xu_yanhai@163.com

Received 15 April 2018; Accepted 10 October 2018; Published 12 November 2018

Guest Editor: Luca Zanotti Fragonara

A railway vehicle's key components, such as wheelset treads and axle box bearings, often suffer from fatigue failures. If these faults are not detected and dealt with in time, the running safety of the railway vehicle will be seriously affected. To detect these components' early failure and extend their fatigue life, a regular maintenance becomes critical. Currently, the regular maintenance of axle box bearings mainly depends on manual off-line inspection, which has low working efficiency and precision of fault diagnosis. In order to improve the maintenance efficiency and effectiveness of railway vehicles, this study proposes a method of integrating the vibration monitoring system of the axle box bearing in the underfloor wheelset lathe, where the integration scheme and work flow of the system are introduced followed by the detailed fault diagnosis method and application examples. Firstly, the band-pass filter and envelope analysis is successively performed on the original signal acquired by an accelerometer. Secondly, the alpha-stable distribution (ASD) and multifractal detrended fluctuation analysis (MFDFA) analysis of the envelope signal are performed, and five characteristic parameters with significant stability and sensitivity are extracted and then brought into the least squares support vectors machine based on particle swarm optimization to determine the state of the bearing quantitatively. Finally, the effectiveness of the method is validated by bench test data. The results demonstrated that the proposed method can accomplish effective diagnosis of axle box bearings' fault location and fault degree and can yield better diagnosis accuracy than the single method of ASD or MFDFA.

1. Introduction

A railway vehicle is usually subjected to complex conditions with variable speeds, loading, and temperatures, which unavoidably lead to wear, pitting, and even peeling fault of its core components, such as wheel treads and axle box bearings (Figure 1) [1–3]. These failures will not only reduce its ride comfort and service life but also impair its safety that may cause serious economic losses or catastrophic casualties, as well as the formation of negative social influence. In August 2007, there was a train derailment accident in Zhengzhou City, Henan Province, China. After investigation, it was concluded that the accident was due to a failure of axle box bearing extending to the axle fracture, eventually leading to the train derailment. In July 2008, an ICE3 high-speed train rated for 330 km/h service speed derailed during departure from Cologne, Central Station, Germany, due to fatigue failure of one of the driving axles. In November 2012, an axle box bearing of a train suddenly broke down whose temperature rose to about 200°C in a very short time, and a lot of burning smell came out. This accident detained the train for a long time and caused a huge economic loss [4, 5]. Therefore, it is necessary to diagnose and process these faults in time.

Currently, the reparation of wheel tread and the fault detection of the axle box bearing are carried out separately. An under-floor wheelset lathe (UWL) is usually applied to

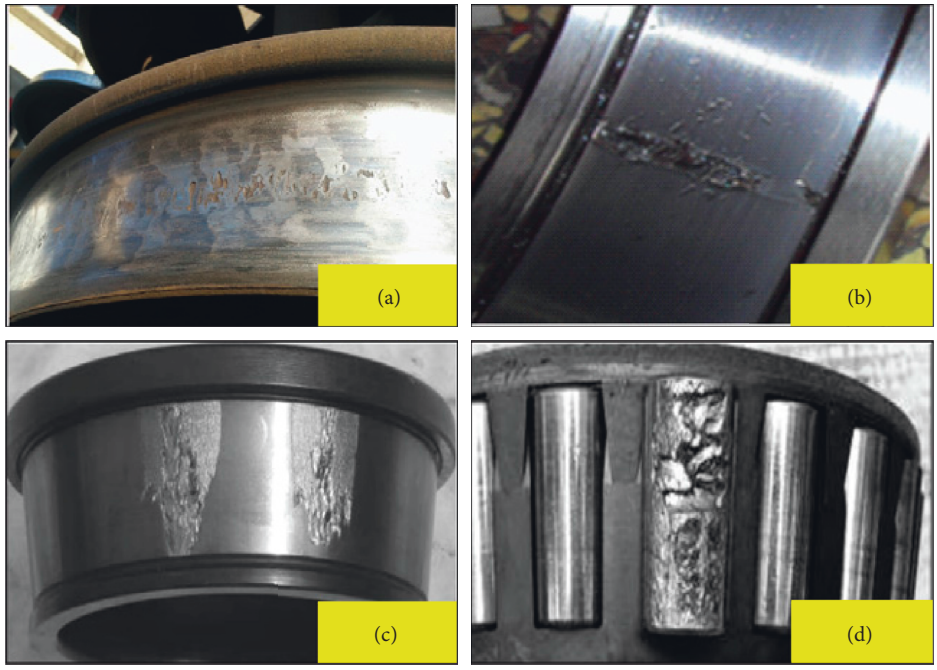

Figure 1: Common localized faults of wheel tread and axle box bearing: (a) failure on wheel tread; (b) failure on the outer race of bearing; (c) failure on the inner race of bearing; (d) failure on the ball of bearing.

regularly maintain railway vehicles and repair its wheel tread failure, since UWL can profile the wheel tread with faults precisely when the wheel set is not broken down [6]. However, the regular maintenance of axle box bearings mainly depends on manual off-line inspection, which has low working efficiency and precision of fault diagnosis due to heavy weight and small assembly space along with several steps of process [7].

The maintenance period is usually formulated by the manufacturer and related to the type and speed level of the railway vehicles. Generally, the profile period of wheel treads is about 200 thousand kilometers [8], and the maintenance period of axle box bearings is generally from one million kilometers [9]. If bearing maintenance and tread repair happen at the same time, the maintenance period of axle box bearings can be shortened and thus the cost can be reduced. Secondly, when the UWL works, the wheel will rotate at a low speed that provides objective conditions of bearing fault diagnosis by monitoring its vibration. Also, this method can reduce the manual intervention which is expected to further improve the diagnostic accuracy and efficiency.

This study proposes the applicable method of integrating the fault diagnosis system of axle box bearings based on vibration monitoring with UWL. Without changing the original structure and function of UWL, this method can diagnose the common faults of axle box bearings. It is different from the current working mode that UWL can only deal with tread damage, and it is of great significance to improve and enrich the existing vehicle maintenance strategy. Meanwhile, the installation of the fault diagnosis system of axle box bearings on UWL has definite engineering background and wide application prospect. It not only increases a maintenance opportunity of bearings which is beneficial to the early detection and prediction of the bearings' faults more accurately but also improves the operation efficiency of the railway vehicle and the economic benefits of the railway business.

2. Integrated Strategy

2.1. System Workflow. An UWL, as illustrated in Figure 2, is composed of a frame, a track system, a positioning device, a parameter measuring device, a supporting device, a clamping device, a profiling device, and a numerical control system [10]. The system workflow that integrates the bearings' fault diagnosis with UWL is shown in Figure 3.

The proposed system workflow has specific steps as follows:

(1) In the interaction of the clamping device, supporting device, and driving friction wheels, the measured wheel is firmly fixed in the center position of UWL.

(2) The parameter measuring device measures the size parameters of the wheelset, such as wheel diameter, wheel inner distance, wheel flange thickness, and wheel flange height. Then, the numerical control system calculates these parameters to form the optimum profiling strategy.

(3) Under the action of two driving friction wheels, the wheelset begins to rotate and reaches a predetermined speed. Then, the profiling device is raised and repair starts.

(4) After one profiling work, the device measures the relevant parameters again. If the parameters are still

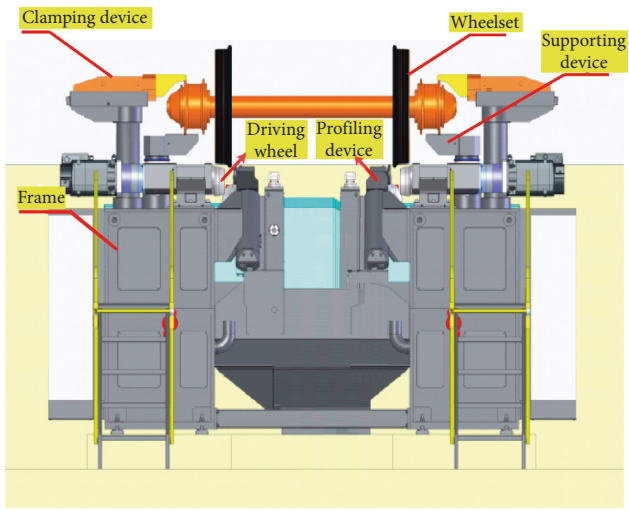

Figure 2: Underfloor wheelset lathe.

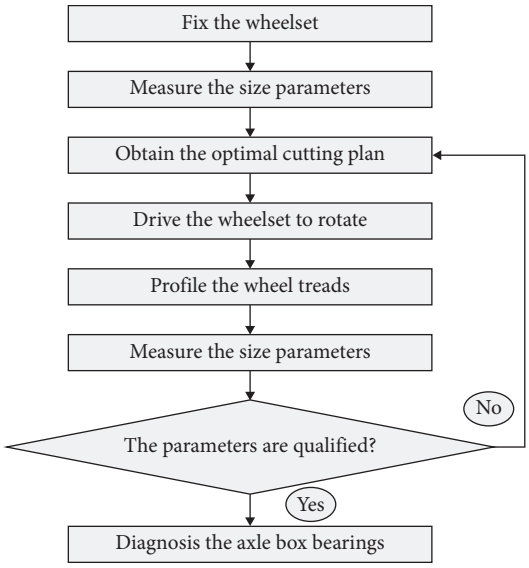

Figure 3: System workflow.

unqualified, go back to step (2) until all parameters are qualified.

(5) When all parameters are qualified, put down the profiling tool. At the same time, let the wheelset continue to rotate and enter the fault diagnosis stage of axle box bearings.

2.2. The Process of Fault Diagnosis for Axle Box Bearings. In order to ensure the profiling quality, the profiling speed is usually between 30 and 120 m/min [11] when the wheel tread is repairing. According to the standard wheel diameter of 0.84 m [12], the corresponding wheel speed can be calculated as about 12 to 46 r/min. At such a low speed, it is very difficult to identify the bearing faults stably and efficiently.

In practical application, the envelope spectrum analysis is the most common method for fault diagnosis of rolling bearing. But this method has the following drawbacks [13, 14]. First, at low-speed conditions, the fault frequency of the bearing is very small that can easily be disturbed by environmental noise. Especially for minor faults, the results of spectrum analysis are poor and the omission judgment occurs sometimes; second, this method can only distinguish fault locations qualitatively but cannot analyze the fault degrees quantitatively.

Therefore, in order to achieve the accurate diagnosis of axle box bearings on UWL, in addition to the envelope spectrum method, this paper also adopts a quantitative method based on alpha-stable distribution (ASD) and multifractal detrended fluctuation analysis (MFDFA).

The widely used ASD has good robustness in the modeling of pulse shape in non-Gaussian signals [15]; MFDFA is able to characterize the internal dynamics mechanism of the fault signal and to detect slight changes in the complex environment of rotating machinery [16]. In References [17, 18], we have studied the sensitivity and stability on fault degrees of the characteristic parameters extracted by ASD and MFDFA, respectively. The results show that the three ASD parameters (the characteristic exponent α, the scale factor γ, and the peak value of the probability density function H) and the two MFDFA parameters (the singularity exponent of the pole h_{q0} and the minimum singularity exponent h_{qmin}) have excellent sensitivity and stability and can be used as the fault characteristics to distinguish the rolling bearings' faults with different locations and degrees.

In summary, this paper will further explore the practicality of the five characteristic parameters (shown in Figure 4) at low speed and aims to realize the intelligent diagnosis of axle box bearings' faults with different locations and degrees on UWL.

The fault diagnosis system of axle box bearings consists of an accelerometer, a speed sensor, a data acquisition device, a communication line, and a high-performance computer (including analysis software). The specific process of the fault diagnosis shown in Figure 5 can be described as follows:

(1) *Signal Acquisition.* Connect the devices as shown in Figure 5. The two acceleration sensors are affixed to the left and right clamping devices of the UWL by two magnetic bases. The speed sensor we selected is a noncontact photoelectric one which must be arranged close to the wheel and need to face the reflective label on the wheel. Subsequently, the output signals of all sensors are collected and processed by the data acquisition device and then communicated to the high-performance computer through the OPC protocol. It is worth noting that the acceleration sensors are mounted on the clamping devices rather than on the axle boxes. Such arrangement can improve the maintenance efficiency because there is no need to rearrange the sensors when replacing wheel sets. Furthermore, this arrangement is easy to install because the material of the clamping device is steel and the upper surface of

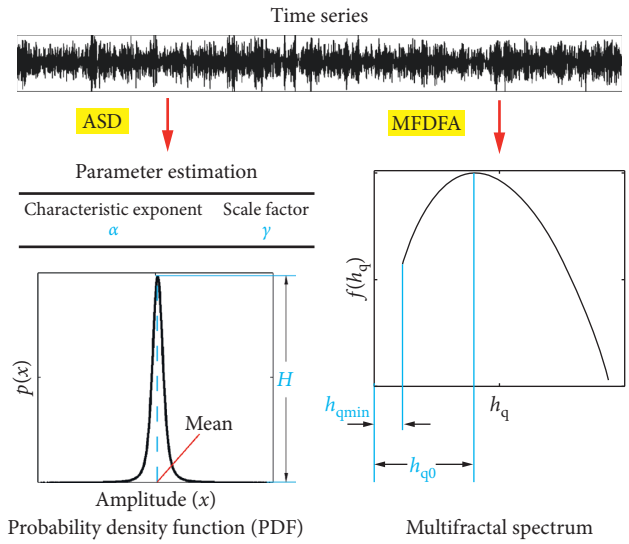

Figure 4: The five characteristic parameters extracted by ASD and MFDFA.

clamping device is smooth enough to arrange the magnetic base conveniently.

(2) *Signal Processing.* The band-pass filter is performed on the original signal obtained by acquisition, and then the envelope analysis is carried out.

(3) *Fault Diagnosis.* The ASD and MFDFA analyses of the envelope signal are carried out, and five fault characteristic parameters (α, γ, H, h_{q0}, and h_{qmin}) are extracted into the PSO-LSSVM model (least squares support vectors machine based on particle swarm optimization) which has been well trained to determine the state of the bearing quantitatively.

It should be noted that the PSO-LSSVM model in Step (3) above needs to be established and trained before the bearing fault diagnosis begins. The detailed process of building the PSO-LSSVM model (shown in Figure 6) is as follows:

(1) Under the working speed of UWL, n status of vibration signals of axle box bearings are obtained as training samples, including normal, inner-race faults (different fault degrees), outer-race faults (different fault degrees), and ball faults (different fault degrees), and labeled as S1, S2, S3, ... Sn, respectively

(2) All signals are band-pass filtered and analyzed by envelope analysis to extract envelope signals

(3) Take ASD and MFDFA analyses on all the envelope signals and extract five fault characteristic parameters (α, γ, H, h_{q0}, and h_{qmin})

(4) Consider the five parameters (α, γ, H, h_{q0}, and h_{qmin}) as input samples and optimize the regularization parameter λ and kernel parameter σ of LSSVM by PSO

(5) Establish the PSO-LSSVM model based on the optimal parameters λ and σ

3. Applications

3.1. Data Acquisition and Processing. In order to further prove the effectiveness of the method proposed in this study, we have carried out the fault setting test of axle box bearings on UGL-type UWL (Figure 7(a)) in Hefei Rolling Stock Depot of Shanghai Railway Administration.

The test bearings are double row cylindrical roller bearings (NJ(P)3226X1) which are widely used in the axle box of railway vehicles. The geometrical parameters of the bearings are shown in Table 1.

Jining mould company in Shandong Province provided the test bearings with the precise machining to achieve seven faults with different locations and degrees, as shown in Figure 8. Every fault location consists of two degrees: slight faults (the width is 5 mm and the depth is 1.5 mm) and serious faults (the width is 10 mm and the depth is 2.0 mm).

When the UWL is running, the wheel speed is 45 r/min. In other words, the outer race of the axle box bearing is fixed, while the inner race of the axle box bearing rotates with the rotational frequency of 0.75 Hz; and the load of the axle box is 80 kN. The acceleration sensor affixed to the clamping devices of the UWL is instrumented to collect vibration signals (Figure 7(b)), with the sampling frequency of 25.6 kHz.

Through experiments, we obtain seven kinds of vibration acceleration signals with different fault locations and different fault degrees of axle box bearings. The fault labels and sizes of seven signals are shown in Table 2.

Figure 9(a) illustrates the gathered first half-second acceleration time histories associated with the seven states of axle box bearing. As we can see from the graph, the seven states cannot be distinguished only by original waveforms.

In order to remove low-frequency noise and enhance the periodic signals which contain fault information, the band-pass filtering is performed on the original signals. According to the document [19] and combined with our repeated experimental experience, we select a 500 to 10 kHz band-pass filter. Then, all filtered signals are subjected to the envelope detector, and seven kinds of envelope signals are obtained as shown in Figure 9(b). Since the Hilbert transformation is used to demodulate the signal in the envelope analysis, the amplitude unit of the envelope signal is dimensionless [20].

Compare the two figures shown in Figures 9(a) and 9(b), we can find that, after band-pass filtering and envelope analysis, the impact characteristics hidden in the signals appear. However, it is still impossible to judge the states of the bearings directly through these signals.

3.2. The Quantitative Diagnosis Method Based on ASD and MFDFA. In order to reduce the randomness of operation, we collected the data length of 3 minutes in each state and divided each data set evenly into 20 segments. Since the wheel speed is 45 r/min, the axle box bearing rotating a revolution needs 1.333 (60/45) seconds and has 34125 (1.333 × 25600) points. The length of total data is 4608000 (25600 × 60 × 3) points, and each segment has 230400

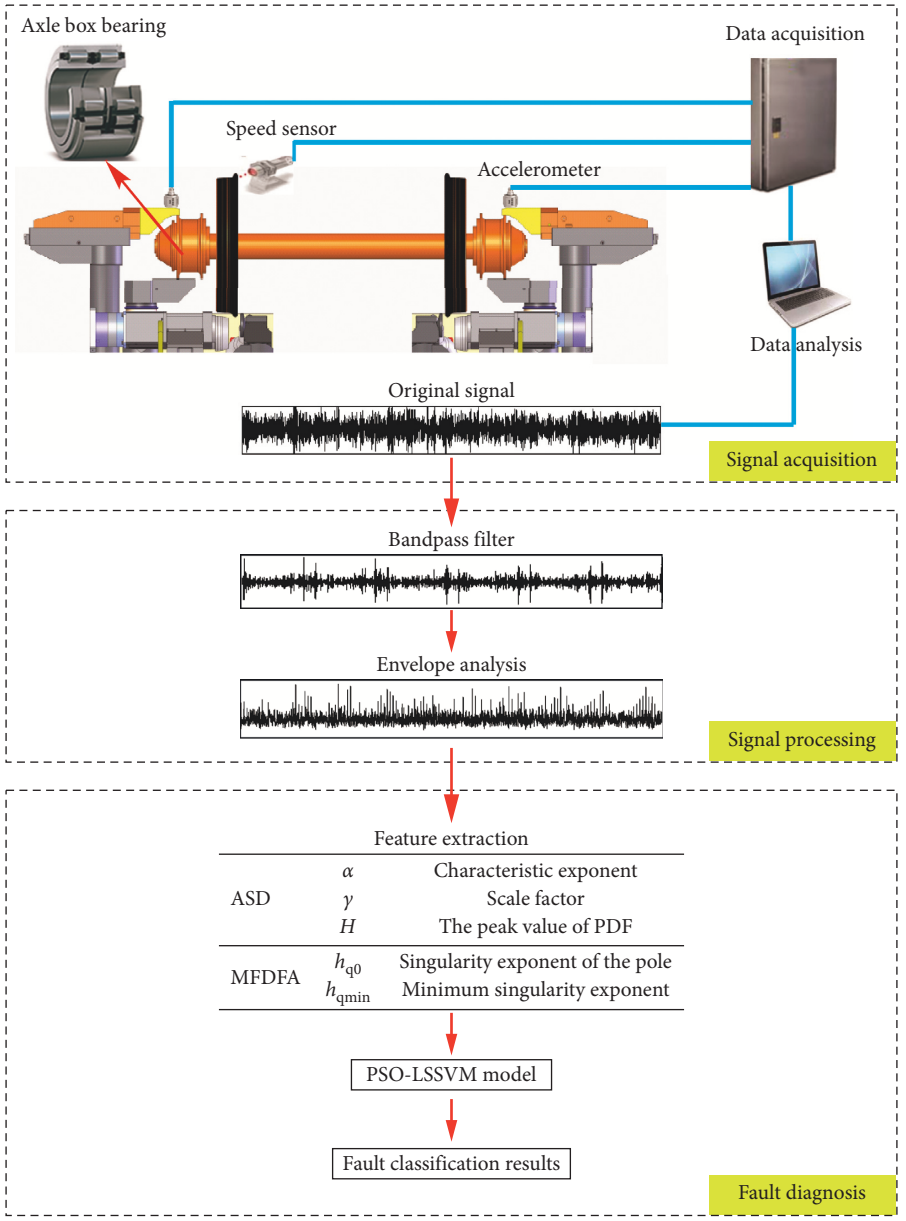

Figure 5: The process of fault diagnosis for axle box bearings.

(4608000/20) data points, so there are about 7 (230400/34125) circles that can be rotated for bearing. According to our experience, the fault information in each segment is enough for further analysis.

Then, 10 segments in each state were randomly selected for training samples and the remaining 10 segments as validation samples. Hence, the total number of training and validation samples is both 70, respectively.

Take ASD analysis and MFDFA analysis on the 70 training samples, the values of five fault characteristic parameters (α, γ, H, h_{q0}, and h_{qmin}) are extracted as shown in Table 3. After averaging, the probability density functions (PDFs) and the multifractal spectrums of each state can be gained, as shown in Figures 10 and 11, respectively.

From Figure 10, we can see the size, shape, and location of PDFs of the seven signals are different, and also there are clear distinction in parameter H. It illustrates that the seven signals have different statistic characteristics. Similarly, from Figure 11, we can see the size, shape, and location of multifractal spectrums of seven signals are different, and also there are clear distinction in parameters h_{q0} and h_{qmin}. It illustrates that the seven signals have different potential dynamics mechanism and multifractal characteristics.

It can be seen from Table 3 that, in different states, the values of the five parameters for each state are inequable. It is worth noting that the four fault characteristic parameters α, H, h_{q0}, and h_{qmin} have the same regularity which can be applied to discern whether there is a fault in the axle box bearing (failure < normal) and also to depict the fault degree under the same fault location (serious faults < slight faults). It is also important to note that the value of γ can be applied to discern whether there is a fault in the axle box bearing

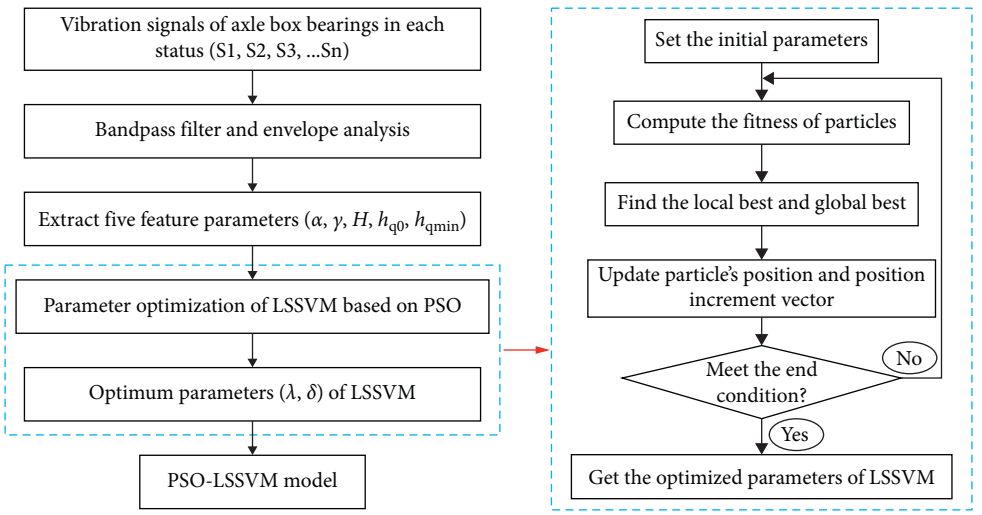

Figure 6: The detailed process of building the PSO-LSSVM model.

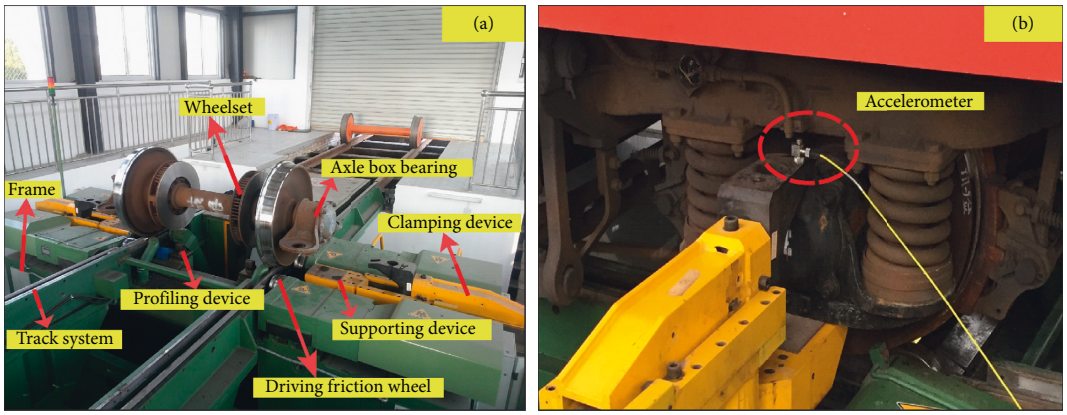

Figure 7: Experimental setup. (a) UGL-type underfloor wheelset lathe; (b) the installation location of the acceleration sensor.

Table 1: Geometrical parameters of the bearings.

Axle box bearing	Outside diameter (mm)	Inside diameter (mm)	Pitch diameter (mm)	Thickness (mm)	Ball diameter (mm)	Ball thickness (mm)
NJ(P)3226X1	250	130	190	80	32	52

(failure > normal) and also to depict the fault degree under the same fault location (serious faults > slight faults).

In order to show the stability and sensitivity for fault quantitative expression of these parameters more clearly, the data of each column in Table 3 graphically expressed are shown in Figures 12(a)–12(e).

Figures 12(a) and 12(d) demonstrate that the values of α and h_{q0} do not change significantly which may indicate that the two parameters can be stably determined from each divided sample data set for all considered bearing states. However, in Figures 12(b), 12(c), and 12(e), the parameter fluctuations of some states are relatively large, especially for the serious outer-race fault states in Figure 12(b) and normal states in Figures 12(c) and 12(e), which may indicate that the stability of parameters γ, H, and h_{qmin} is relatively poor compared with that of the other two parameters. Regarding the parameter sensitivity, significant value differences can be seen between each other for all state curves in all Figures 12(a)–12(e), and such value differences are enough to distinguish the seven states, which indicates the sensitivity of all the five fault characteristic parameters (α, γ, H, h_{q0}, and h_{qmin}) are significant in every state.

The above analysis proves that the five characteristic parameters (α, γ, H, h_{q0}, and h_{qmin}) selected in this paper can quantitatively reflect the fault degree of the axle box bearings. If these parameters are combined with an appropriate classification method, the intelligent diagnosis of the axle box bearings on UWL may be realized.

Therefore, we put the 5D fault characteristic parameters (α, γ, H, h_{q0}, h_{qmin}) = [(α_1, γ_1, H_1, h_{q01}, h_{qmin1}), (α_2, γ_2, H_2, h_{q02}, h_{qmin2}), . . ., (α_{10}, γ_{10}, H_{10}, h_{q010}, h_{qmin10})] obtained in Table 3 into the PSO-LSSVM model for training. The

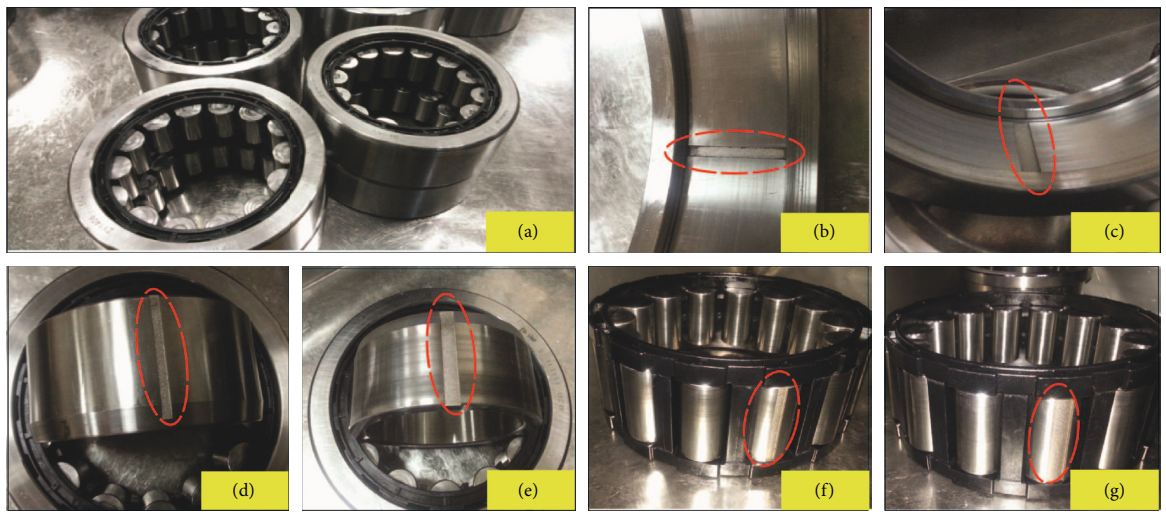

Figure 8: Artificial faults on the components of the axle box bearing: (a) normal; (b) slight outer-race faults; (c) serious outer-race faults; (d) slight inner-race faults; (e) serious inner-race faults; (f) slight ball faults; (g) serious ball faults.

Table 2: The detail descriptions of seven vibration acceleration signals.

Label	Running state	Fault width (mm)	Speed (r/min)	Sampling frequency (kHZ)	Load (kN)
S1	Normal	0	45	25.6	80
S2	Slight inner-race faults	5	45	25.6	80
S3	Serious inner-race faults	10	45	25.6	80
S4	Slight outer-race faults	5	45	25.6	80
S5	Serious outer-race faults	10	45	25.6	80
S6	Slight ball faults	5	45	25.6	80
S7	Serious ball faults	10	45	25.6	80

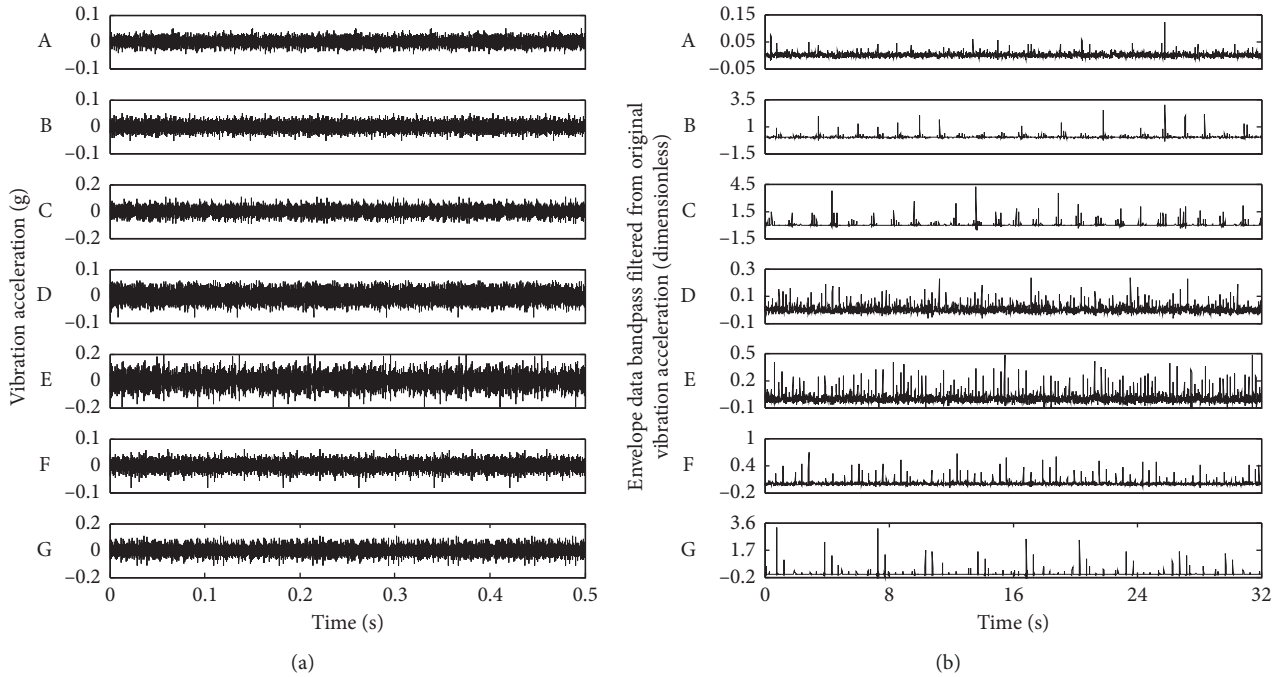

Figure 9: The waveforms of seven vibration acceleration signals. (a) Original signal. (b) Envelope signals.

Table 3: The detailed descriptions of seven vibration acceleration signals.

Operational status	α	γ	H	h_{q0}	h_{qmin}
Normal (S1)	1.8993	0.0096	29.4120	1.8457	1.4556
	1.9067	0.0087	29.0582	1.8591	1.5075
	1.9151	0.0089	30.4335	1.8383	1.4541
	1.9094	0.0092	30.9254	1.8247	1.5057
	1.9195	0.0088	30.0025	1.8480	1.4841
	1.9034	0.0095	29.6416	1.8510	1.4693
	1.9052	0.0095	29.7845	1.8449	1.4516
	1.9132	0.0094	30.0323	1.8395	1.4932
	1.9077	0.0093	30.3889	1.8541	1.5014
	1.9023	0.0090	31.1737	1.8451	1.4525
Slight inner-race faults (S2)	1.3320	0.0107	26.1155	1.7160	1.0720
	1.3154	0.0102	25.5469	1.7137	1.0633
	1.3296	0.0101	25.8140	1.7135	1.0638
	1.3230	0.0112	26.1135	1.7087	1.0595
	1.3287	0.0109	26.1692	1.7065	1.0607
	1.3292	0.0104	25.9836	1.7066	1.0590
	1.3172	0.0104	27.0754	1.7176	1.0719
	1.3133	0.0109	26.2662	1.7060	1.0611
	1.3212	0.0111	26.0422	1.7197	1.0644
	1.3164	0.0115	26.3823	1.7269	1.0789
Serious inner-race faults (S3)	0.7018	0.0151	19.4513	1.6388	0.9678
	0.6925	0.0144	18.1511	1.6445	0.9641
	0.6956	0.0149	18.9960	1.6459	0.9738
	0.7049	0.0152	18.8235	1.6483	0.9577
	0.6841	0.0146	19.9549	1.6394	0.9867
	0.6898	0.0144	19.9818	1.6560	0.9787
	0.6985	0.0152	20.1924	1.6455	0.9669
	0.6819	0.0153	19.1857	1.6498	0.9629
	0.6900	0.0150	19.8159	1.6552	0.9838
	0.6961	0.0156	19.4017	1.6496	0.9741
Slight outer-race faults (S4)	1.5162	0.0158	17.6917	1.5515	1.2857
	1.5307	0.0158	17.7755	1.5296	1.2828
	1.5223	0.0164	17.7314	1.5451	1.3100
	1.5254	0.0158	17.7576	1.5231	1.3149
	1.5047	0.0159	17.7512	1.5361	1.2986
	1.5282	0.0161	17.5879	1.5306	1.2912
	1.5093	0.0158	17.8053	1.5216	1.2982
	1.5190	0.0159	17.7555	1.5507	1.3040
	1.5242	0.0161	17.6028	1.5440	1.3017
	1.5221	0.0162	17.5019	1.5411	1.2853
Serious outer-race faults (S5)	1.4205	0.0188	15.1236	1.4037	1.1938
	1.4250	0.0186	15.2996	1.3930	1.2019
	1.4322	0.0181	15.0908	1.3960	1.2091
	1.4158	0.0186	15.1885	1.3908	1.1998
	1.4307	0.0187	15.1936	1.3810	1.2067
	1.4247	0.0185	15.3594	1.3926	1.2138
	1.4193	0.0177	16.1091	1.3934	1.1992
	1.4096	0.0193	15.7148	1.3824	1.2013
	1.4166	0.0193	15.7449	1.3909	1.2060
	1.4202	0.0191	15.8696	1.3758	1.1869
Slight ball faults (S6)	1.5929	0.0121	23.1508	1.6817	1.3872
	1.6082	0.0119	23.4960	1.6839	1.3865
	1.6002	0.0121	23.2410	1.6746	1.3822
	1.5919	0.0119	23.6557	1.6863	1.3884
	1.5844	0.0123	22.9531	1.6848	1.3910
	1.5880	0.0120	23.4184	1.6831	1.3833
	1.5999	0.0121	23.1717	1.6728	1.3847
	1.5890	0.0117	24.0167	1.6733	1.3857
	1.6057	0.0120	23.3415	1.6825	1.3832
	1.5960	0.0123	22.8547	1.6835	1.3765

Table 3: Continued.

Operational status	α	γ	H	h_{q0}	h_{qmin}
Serious ball faults (S7)	1.3643	0.0203	12.7830	1.4739	1.2476
	1.3555	0.0199	12.9226	1.4870	1.2584
	1.3634	0.0203	13.3643	1.4676	1.2451
	1.3552	0.0210	13.2624	1.4715	1.2599
	1.3583	0.0197	13.4797	1.4755	1.2608
	1.3419	0.0199	14.0001	1.4803	1.2462
	1.3540	0.0205	13.6946	1.4822	1.2461
	1.3492	0.0211	13.3486	1.4821	1.2570
	1.3509	0.0207	13.5415	1.4813	1.2592
	1.3679	0.0215	13.1382	1.4982	1.2529

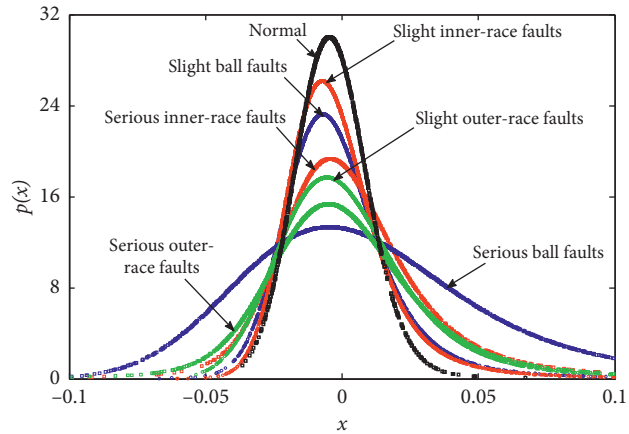

Figure 10: The PDFs of seven signals.

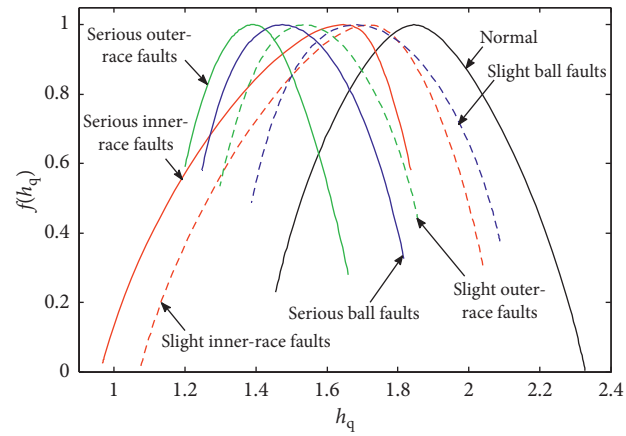

Figure 11: The multifractal spectrums of seven signals.

primary parameters of PSO are shown in Table 4. After iterated operation, we got the optimal parameters for LSSVM: $\sigma = 0.0973$ and $\lambda = 4.1701$.

Meanwhile, we used the remaining ten segments data as the validation samples to extract the five fault characteristic parameters $(\alpha, \gamma, H, h_{q0}, h_{qmin})' = [(\alpha_{11}, \gamma_{11}, H_{11}, h_{q011}, h_{qmin11}), (\alpha_{12}, \gamma_{12}, H_{12}, h_{q012}, h_{qmin12}), \ldots, (\alpha_{20}, \gamma_{20}, H_{20}, h_{q020}, h_{qmin20})]$ and lastly put it into the PSO-LSSVM model which had been trained well to classify. In order to reduce the amount of calculation, we chose the coding method of

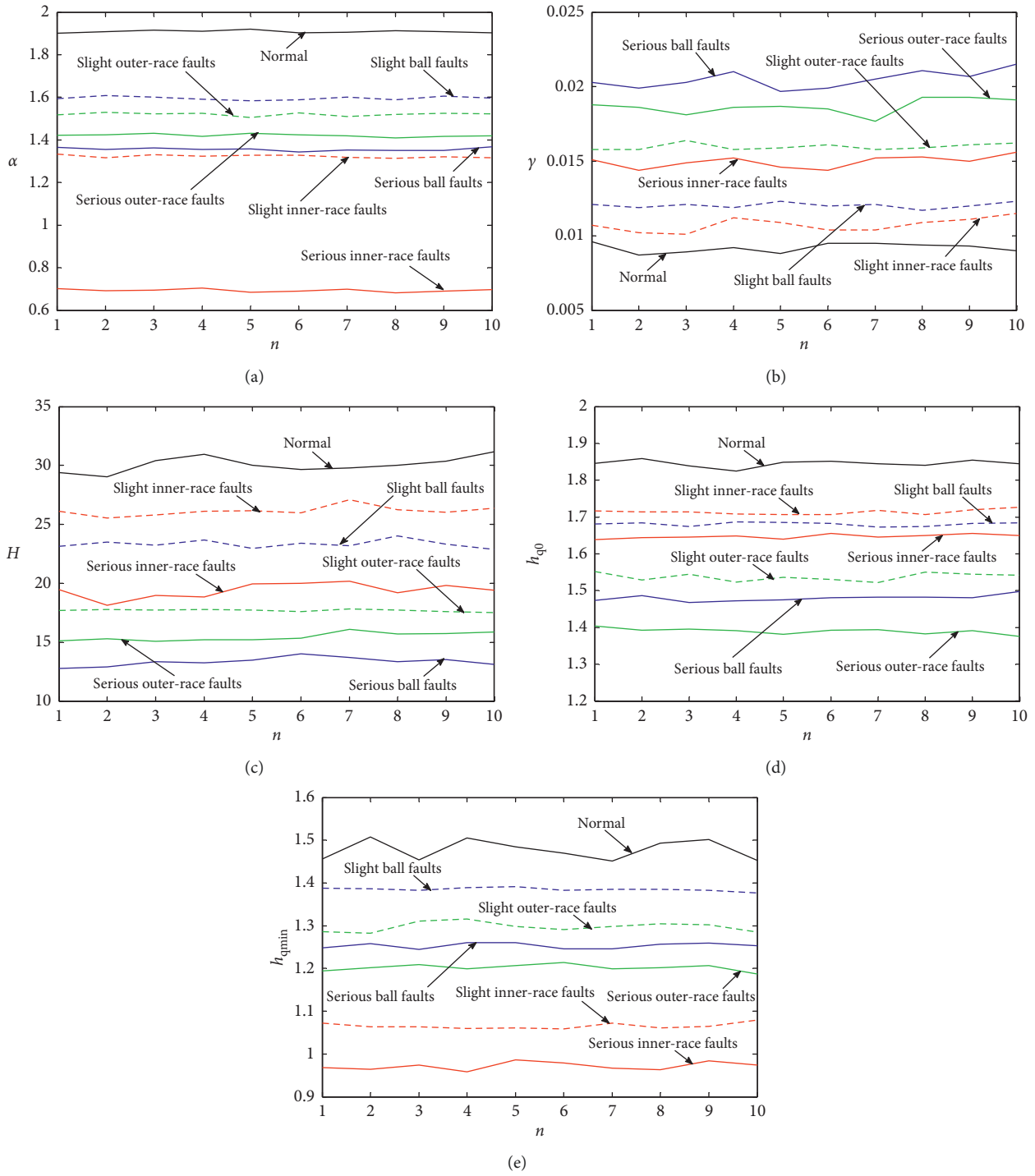

Figure 12: The stability and sensitivity of the five fault characteristic parameters of seven signals. (a) α. (b) γ. (c) H. (d) h_{q0}. (e) h_{qmin}.

Table 4: The primary parameters of PSO.

Parameter	Value
Primary position and its increment vector	Generate randomly
Population size	40
Maximum iteration number	200
Accelerating coefficients c_1 and c_2	2
Optimal range of λ and σ	0.01–100

minimum output coding and adopt three classifiers to meet the requirement of diagnosis.

In order to investigate the advantages of the proposed method, we also built the PSO-LSSVM model based on the 3D ASD characteristic parameters (α, γ, and H) and the 2D MFDFA characteristic parameters (h_{q0} and h_{qmin}), respectively. After decoding, the classification results with three methods are shown in Figures 13–15.

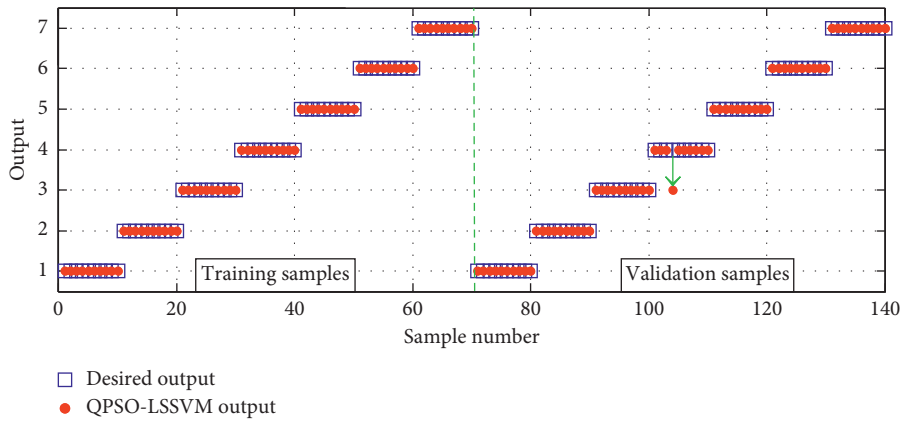

Figure 13: Classification results of the PSO-LSSVM model based on ASD and MFDFA parameters.

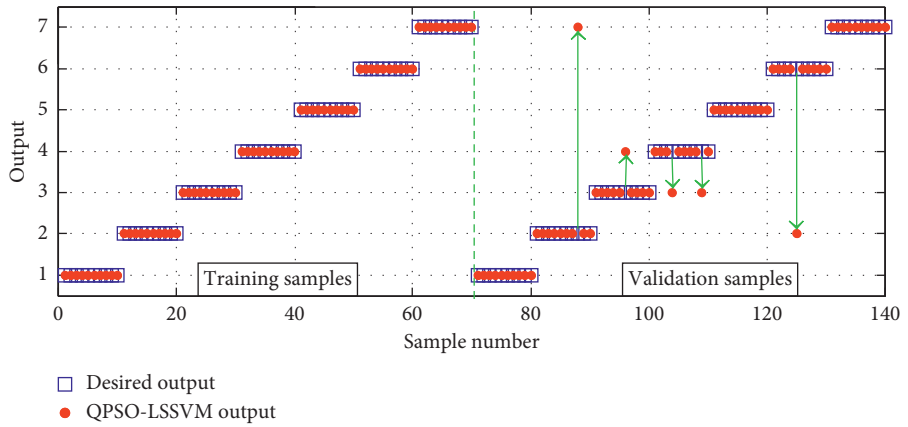

Figure 14: Classification results of the PSO-LSSVM model based on ASD parameters.

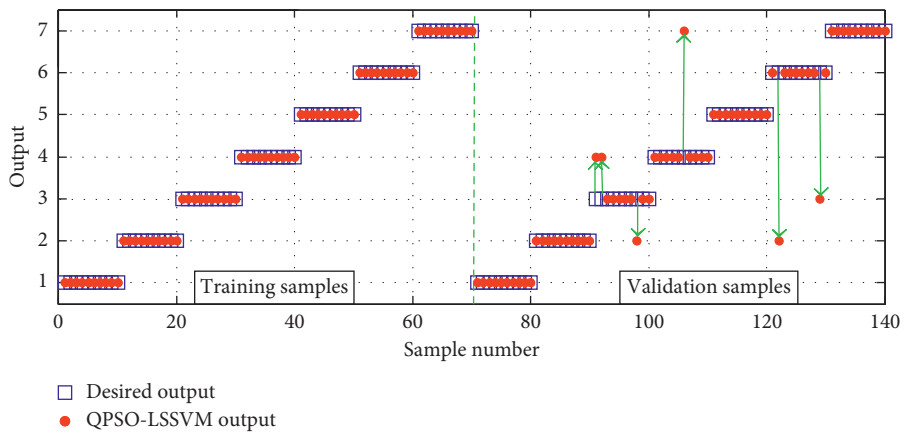

Figure 15: Classification results of the PSO-LSSVM model based on MFDFA parameters.

It can be seen from Figures 13–15, under the condition of training samples and validation samples are both 70, all the above three methods can distinguish the states of the validation samples, though their diagnostic accuracies are different. This once again shows that the five parameters (α, γ, H, h_{q0}, and h_{qmin}) can be used as the fault characteristics to distinguish different fault locations and fault degrees of axle box bearings on UWL.

Regarding the generalization ability, we can see from Figure 13 that the method that combined five parameters (α, γ, H, h_{q0}, and h_{qmin}) with the PSO-LSSVM model has only one mistake; that is, a sample originally belonged to S4 but

was classified under S3 (see the green arrow), and the diagnostic accuracy is 98.6%. Figure 14 shows that the method that combined only three ASD parameters (α, γ, and H) with the PSO-LSSVM model has five green arrows which indicates that there are five mistakes: a sample in S2 is assigned to S7, a sample in S3 is assigned to S4, two samples in S4 are assigned to S3, and a sample in S6 is assigned to S2, and the diagnostic accuracy is 92.9%. Similarly, it also can be seen from Figure 15 that the method that combined only two MFDFA parameters (h_{q0} and h_{qmin}) with the PSO-LSSVM model has six mistakes, and the diagnostic accuracy is 91.4%.

So, the PSO-LSSVM model based on five parameters (α, γ, H, h_{q0}, and h_{qmin}) which is proposed in this paper has the highest diagnostic accuracy. It demonstrated that the combination of the characteristic parameters extracted by ASD and MFDFA can improve their effectiveness and enhance the recognition ability of the classifier; hence, the diagnosis accuracy of axle box bearings on UWL can be improved.

4. Conclusions and Future Works

Based on the study, the following conclusions can be drawn:

(1) Through the fault setting experiments, it is proved that the idea of integrating the fault diagnosis system of axle box bearings based on vibration monitoring with UWL is feasible and practically applicable.

(2) The method that combined the five ASD and MFDFA parameters (α, γ, H, h_{q0}, and h_{qmin}) with the PSO-LSSVM model can effectively distinguish the seven signals with different fault locations and fault degrees of axle box bearings on UWL, and its diagnostic accuracy is higher than the single method of ASD or MFDFA.

There may be some achievable directions for next works. Firstly, this study has classified the states of axle box bearings into only seven classes under the circumstance of small samples, and thus more samples should be supplemented with various health states to further test its capability for multiclassifications. Then, the accelerated fatigue life tests of axle box bearings may be implemented to obtain the acceleration signals of all phases (normal, fatigue, and failure) of the bearings' life cycle so as to form the failure feature sequences and set the failure thresholds of the bearings, which could be combined with the grey model, the support vector machine, or the random filter to predict the residual lives of the bearings.

Secondly, the faults in this study were generated artificially which contains only a single fault in a bearing. However, axle box bearings often have faults at different locations at the same time in practice, which is called compound faults. To further enhance the engineering application value of the proposed method, enough samples with compound faults of axle box bearings should be supplemented to validate its effectiveness. On the basis of signal denoising, the different features of compound faults may be separated by the signal decomposition methods (such as wavelet transform, empirical mode decomposition, or their improved methods) combined with the blind source separation method (such as independent component analysis). Then, the signals after separation could be fed to the proposed method in this paper to realize the diagnosis of compound faults.

Data Availability

The vibration acceleration data of axle box bearing used to support the findings of this study are obtained by our own experiments. In order to obtain these data which contain different fault locations and fault degrees of axle box bearings, our two units (Xihua University and Southwest Jiaotong University) experienced the process of connecting manufacturers (Hefei Rolling Stock Depot of Shanghai Railway Administration and Jining mould company in Shandong Province), purchasing bearings, setting up faults, upgrading test rig, hiring testers, bench test, and so on. Especially in the bench test, because the manufacturers have their own production and maintenance tasks, we can only take experiments in spare time. Moreover, the dismantling, replacement, cleaning, marking, and other work of axle box bearing must comply with the manufacturer's working time flow, so the whole test took more than half a year, and we had spent a lot of time, money, and labor. Therefore, the data in this paper cannot be open to the public free of charge. If there is any need, contact the corresponding author via e-mail. If our two units (Xihua University and Southwest Jiaotong University) are licensed, these data can be provided.

Conflicts of Interest

The authors declare that there are no conflicts of interest regarding the publication of this paper.

Acknowledgments

This work was supported in part by the Applied Basic Research Programs of the Science and Technology Department of Sichuan Province (2018JY0238), the Major Project of Education Department in Sichuan Province (17ZA0354), the National Nature Science Foundation of China (51775448), the Project of Spring Plan of the Ministry of Education (Z2012024), the Science and Technology Research and Development Program of Sichuan Province (2017GZ0103), the Open Research Subject of Key Laboratory of Fluid and Power Machinery (Xihua University), Ministry of Education (szjj2016-013), the Open Research Subject of Key Laboratory of Automotive Measurement, Control and Safety (Xihua University) (szjj2017-078), and the Key Scientific Research Fund Project of Xihua University (z1620303).

References

[1] Y. Li, X. Liang, J. Lin et al., "Train axle bearing fault detection using a feature selection scheme based multi-scale morphological filter," *Mechanical Systems and Signal Processing*, vol. 101, pp. 435–448, 2018.

[2] J. Ding, F. Li, J. Lin et al., "Fault detection of a wheelset bearing based on appropriately sparse impulse extraction," *Shock and Vibration*, vol. 2017, Article ID 7853918, 17 pages, 2017.
[3] Y. Li, J. Liu, and Y. Wang, "Railway wheel flat detection based on improved empirical mode decomposition," *Shock and Vibration*, vol. 2016, Article ID 4879283, 14 pages, 2016.
[4] C. Klinger and D. Bettge, "Axle fracture of an ICE3 high speed train," *Engineering Failure Analysis*, vol. 35, no. 26, pp. 66–81, 2013.
[5] Q. Xiong, *Research on feature extraction and fault diagnosis method of vibration signal of rolling bearing in train*, Ph.D. thesis, Southwest Jiaotong University, Chengdu, China, 2015.
[6] T. Nijssen and H. J. Reiche, "Underfloor wheel set lathe for machining wheel sets of railway vehicles," European Patent, EP1836018, 2007.
[7] J. Zhang and Q. Zhang, "The underfloor wheelset replacement device of axle box bearing in Shaoshan locomotives," *Electric Drive for Locomotives*, vol. 6, pp. 83-84, 2011.
[8] V. C. Tao, L. Fu, Z. Qi et al., "Processing method of locomotive wheel wear statistical data and predication model of turning period," *Journal of the China Railway Society*, vol. 37, no. 12, pp. 14–19, 2015.
[9] H. Sun, "Discussion on bearing service life of passenger electric locomotives," *Railway Locomotive and Car*, vol. 30, no. 6, pp. 88–90, 2010.
[10] L. Cai, G. Sun, and Z. Liu, "The dynamic characteristic and finite element analysis on wheelset driving system of underfloor wheelset lathe," in *Proceedings of 2014 International Conference on Mechanics and Civil Engineering (ICMCE-14)*, pp. 292–298, Wuhan, China, December 2014.
[11] W. Haibo, "The analysis and treatment of common faults of U2000-400 type underfloor wheelset lathe," *Shanghai Railway Science and Technology*, vol. 2, pp. 123–125, 2016.
[12] J. Yan and M. Fu, *Vehicle Engineering*, China Railway Publishing Press, Beijing, China, 3rd edition, pp. 43–46, 2009.
[13] N. Wang, C. Cheng, C. Sun et al., "Study on fault diagnosis of low-speed rolling bearing using stress waves and wavelet analysis," *Journal of Vibration Engineering*, vol. 20, no. 3, pp. 280–284, 2007.
[14] J. Schoukens, Y. Rolain, and R. Pintelon, "Analysis of windowing/leakage effects in frequency response function measurements," *Automatica*, vol. 42, no. 1, pp. 27–38, 2006.
[15] G. Yu, C. Li, and J. Zhang, "A new statistical modeling and detection method for rolling element bearing faults based on alpha-stable distribution," *Mechanical Systems and Signal Processing*, vol. 41, no. 1-2, pp. 155–175, 2013.
[16] J. Lin and Q. Chen, "Fault diagnosis of rolling bearings based on multifractal detrended fluctuation analysis and Mahalanobis distance criterion," *Mechanical Systems and Signal Processing*, vol. 38, no. 2, pp. 515–533, 2013.
[17] Q. Xiong, W. Zhang, T. Lu et al., "Rolling bearing fault diagnosis based on parameter estimate of alpha-stable distribution," *Journal of Vibration, Measurement and Diagnosis*, vol. 35, no. 2, pp. 238–244, 2015.
[18] Q. Xiong and Z. Weihua, "Rolling bearing fault diagnosis method using MF-DFA and LSSVM based on PSO," *Journal of Vibration and Shock*, vol. 34, no. 11, pp. 188–193, 2015.
[19] X. He, F. Dai, Z. Su et al., "Fault diagnosis of rolling bearing based on acceleration envelope technique," *China Plant Engineering*, vol. 10, pp. 63–65, 2017.
[20] Y. T. Sheen, "On the study of applying Morlet wavelet to the Hilbert transform for the envelope detection of bearing vibrations," *Mechanical Systems and Signal Processing*, vol. 23, no. 5, pp. 1518–1527, 2009.